Int J Fract (2011) 171:125–137
DOI 10.1007/s10704-011-9631-9

ORIGINAL PAPER

How the obscuration-zone hypothesis affects fragmentation: Illustration with the cohesive-element method

M. Chambart · S. Levy · J. F. Molinari

Received: 13 April 2011 / Accepted: 13 September 2011 / Published online: 18 October 2011

Abstract The problem of fragmentation prediction is at the origin of various analytical models. Among them, we focus on the ones introducing the idea of obscured zones. They assume that when a crack initiates at a defect, a stress release wave propagates away from the crack and protects the region encompassed by the wave from any further crack initiation. In this paper, we show by the use of numerical simulations that this assumption is only valid at high strain rates. The limit of its accuracy is even pushed to higher strain rates when the fragmentation process becomes more complex, that is to say when crack propagation, bifurcation or coalescence together with wave reflections are implied. In these cases, fragmentation lasts longer than the time needed to completely obscure the whole specimen and the obscured zone theory for fragmentation appears inadequate. We use the cohesive-element method to describe the damage and failure of the material considered.

Keywords Fragmentation · Obscured zones · Cohesive zone modeling · Crack propagation

M. Chambart (✉) · S. Levy · J. F. Molinari
L.S.M.S - I.I.C - E.N.A.C, Ecole Polytechnique Fédérale de Lausanne, 1015 Lausanne, Switzerland
e-mail: marion.chambart@epfl.ch

1 Introduction

1.1 Historical background

Fragmentation prediction is a key issue for many industrial applications both from military and civil domains. The list cannot be exhaustive, but includes for instance the design of ceramic light-weight armor, tunnelling, mining or fragmentation of kidney stones. These applications have in common their dynamical aspect, which plays a major role in the fragmentation process.

Fragmentation has been studied for decades, and the evolution of the knowledge on the subject has increased a lot from the first empirical descriptions of Rosin and Rammler (1999). They observed that the distribution of the particle sizes issued from the crushing of coal and other materials follows what will be later called a Weibull distribution Weibull (1951). In Weibull (1939), the author carried out quasi-static experiments and proposed the same distribution. In this article, he introduces the notion of probability for a specimen to break at a given stress. In other words, Weibull first explained that failure occurs at some locations where the material exhibits a weakness, i.e. a defect.

A theory of geometric fragmentation statistics was developed by Lienau (1936) to explain the results obtained by Rosin and Rammler. This theory, using Poisson statistics, predicts the distribution of the length of fragments in a 1D bar. Mott and Linfoot (1943) proposed an extension to 2D, but it was only

in 1985 that Grady and Kipp (1985) were able to solve it numerically and obtain the distribution of fragments size. Other statistical algorithms were later developed, a detailed review can be found in Grady (2006).

However it was clear at this point, that statistics alone were not sufficient to reproduce all the complexity of the fragmentation process. A major step was conducted by Mott (1947), who introduced in his statistical theory, the notion of stress relaxation waves and thus time-dependency of the fragmentation process.

A different alternative theory, based on energy balance principles has also been developed (Grady et al. 1984; Kipp and Grady 1985; Glenn and Chudnovsky 1986), which predicts the average fragment size. Years later, these models pioneered by Grady are still widely used in several applications.

Finally, with the progress of numerical methods, it has become possible to reproduce explicitly the fragmentation process and to propose new fragmentation models that reproduce more accurately the experimental results (Zhou et al. 2006; Levy and Molinari 2010; Morris et al. 2006; Denoual et al. 1997; Donzé et al. 1997; Astrom et al. 2004; Herrman et al. 2006; Maiti et al. 2004; Miller et al. 1996).

1.2 The obscured zone theory

As mentioned before, Mott was the first to formulate a fragmentation model based on the physics of wave propagation. He studied the case of a perfectly plastic ring in dynamical expansion. When fracture occurs, it creates a stress release wave that propagates away from the fracture site. Then, as Grady (2006) summarizes the situation : "*Fracture physics(...) is governed by the competition of waves of release emanating from existing fracture, with continuing fractures occurring within regions of the body not yet subsumed by these waves*", which actually means that no fracture can occur anymore in this region. Hild and coworkers (Denoual et al. 1997; Forquin and Hild 2010) developed on this basis a damage model within a thermodynamic framework. They assume that "*The fragmentation process ends when the whole domain is obscured*". The purpose of this article is to show that this hypothesis is not valid in every situation. Indeed, dynamic loadings imply time-dependency, but also complex phenomena of wave propagation and reflections, as it has been explained for instance in an analysis conducted by Drugan (2001). When a crack appears, a stress release wave propagates and modifies the stress state in the cracked neighborhood. Besides, the crack created can be considered as a new discontinuity in the material. As a consequence, any wave meeting this surface is reflected into an opposite wave of the same intensity. It means that a stress release wave becomes a tensile wave and can either reload a defect that has been initiated but not opened, or initiates an obscured defect. We call these waves *secondary waves*. Due to inertial effects, the tensile stress can even be higher than the one that caused the first crack opening. As a consequence, the number of fragments is in the end more important that the one predicted by the obscured zone models. Furthermore, in 2D or 3D, a fragment is the result of a complex process involving not only initiation but also propagation and coalescence of cracks. This process takes more time than needed to completely obscure the whole specimen.

In this article, we propose to use a numerical finite-element model that explicitly represents the cracks and thus the fragments to study the domain of validity of the obscured zone theory. Focus will be put on the influence of different parameters: strain rate, distribution of defects, brittleness, dimension of the problem (1D/2D) and the loading states (uniaxial/biaxial).

The cohesive zone method employed to model fracture is described in the second section of the article, along with the implementation of the obscured zones hypothesis. Then a first example, a 1D bar in uniaxial extension is presented in order to illustrate the influence of secondary waves on crack initiation. One can observe that at high strain rates, this influence is insignificant while, for lower strain rates, the observed results can differ importantly. The fourth part tackles the problem of crack propagation in 2D. In that case, we can show that the obscured zone hypothesis prevents the generation of fragments, especially at low strain rates and under uniaxial tension. Finally, the fifth part shows on a 2D plate in biaxial tension, that the more distributed the defects are, the more influent the obscured zone theory is. The same effect is observed if the brittleness increases.

2 Numerical modeling of fracture and obscured zones

2.1 Cohesive zone modeling

The different examples presented in this article are computed using a finite-element code. They are conducted in 2D in order to reduce the computation cost and thus to conduct larger parametric studies. The body is discretized into 6-noded triangles. The model is linear elastic until failure. The discretization in time is based on an explicit central difference scheme (Hughes 2000). The stable time step is computed at the beginning of the simulation. It is defined by:

$$\Delta t = S\frac{\min(h_e)}{c} \tag{1}$$

$c = \sqrt{\frac{E}{\rho}}$ is the longitudinal wave speed and h_e is a characteristic length computed for each element. Since the stable time step is computed before any loading is applied and and since the elements may deform, a security factor S is applied, usually 0.1.

The failure behavior is controlled by cohesive elements. They describe the softening behavior of the material and are not present at the beginning of the computation. They are introduced dynamically as in Camacho and Ortiz (1996). This method is called the extrinsic approach, in opposition to the intrinsic approach where the cohesive elements compose together with the bulk elements the initial mesh. Two solutions are possible with the latter method: either the cohesive elements are placed where cracking is supposed to happen or they are put everywhere. The first option implies to be able to predict a priori the crack pattern, which limits the possible studies to really simple ones. The second one has the drawback to modify the global elastic properties of the material. Indeed, the elements need to have an initial stiffness, that unless it is infinite, influences the global one. The drawback is that it reduces drastically the stable time step. As a consequence, in intrinsic approaches, a medium stiffness is usually chosen and the global wave speed is modified. The problem for dynamic applications is then obvious.

In extrinsic approaches, a threshold in stress controls the initiation of damage (i.e., the insertion of cohesive elements). Here, we compute the average normal stress at each interface between two bulk elements. When this stress reaches the critical stress σ_c, we duplicate the nodes at the interface in order to introduce the cohesive element (see Fig. 1).

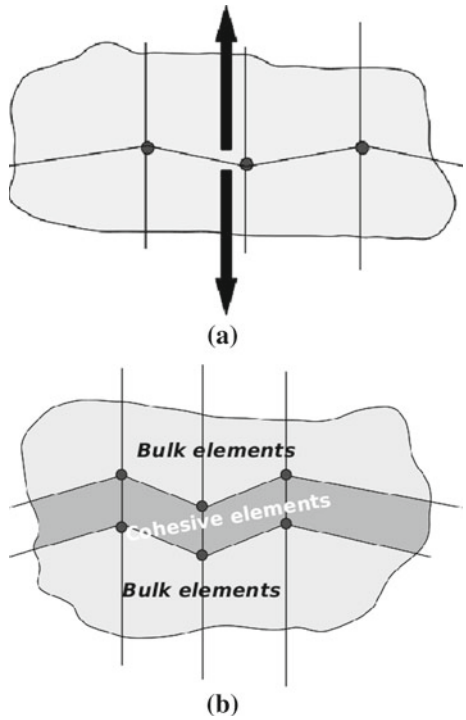

Fig. 1 (**a**) Before cohesive elements insertion, (**b**) after insertion. Dynamic insertion of cohesive elements (or extrinsic approach) Camacho and Ortiz (1996)

The softening behavior follows a linear decreasing cohesive law, which relates the local stress σ_{coh} and the opening displacement δ_{coh} (Fig. 2). The cohesive law is:

$$\frac{\sigma_{coh}}{\sigma_c} = 1 - \frac{\delta_{coh}}{\delta_c} \quad \text{for } \delta_{coh} = \delta_{\max} \text{ (first loading)}. \tag{2}$$

$$\sigma_{coh} = \frac{\sigma_{\max}}{\delta_{\max}}\delta_{coh} \quad \text{for } \delta_{coh} < \delta_{\max}$$

(unloading or reloading). (3)

The damage variable D is defined as the ratio between the maximum opening displacement and the critical displacement.

$$D = \frac{\delta_{\max}}{\delta_c} \tag{4}$$

The energy associated to fracture is divided into a dissipated part E_d and a recoverable part E_r. When a cohesive element is completely broken, all the dissipable energy has been released. It corresponds to the toughness G_c, the area under the stress opening law. It can

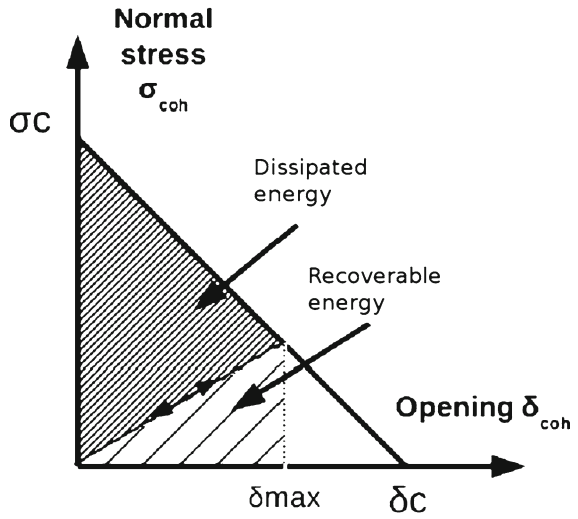

Fig. 2 The linear cohesive law and the associated energies Camacho and Ortiz (1996)

be written $G_c = \frac{1}{2}\sigma_c\delta_c$. When it is partially opened ($D < 1$), the dissipated energy is:

$$E_d = DG_c \tag{5}$$

and the recoverable energy is:

$$E_r = (1 - D)DG_c \tag{6}$$

2.2 A numerical method to reproduce the obscured zones

The extrinsic approach described in the previous section offers a simple opportunity to model the obscured zone hypothesis. Indeed, each interface (edge) between two elements is a potential crack initiation site and can be therefore considered as a defect. The obscured zone theory states that, if a stress release wave passes through a defect, then this defect is protected from any further nucleation. Numerically, one way to reproduce this hypothesis is to make unbreakable any edge where a decrease in the normal stress is measured. The stress is considered as decreasing if its difference between two consecutive time steps exceeds the threshold 0.1 MPa. This value has been chosen to be above numerical instabilities. The fragmentation process and the computation end when all the domain is obscured. The edges are either partially damaged, fully broken, or deactivated.

Table 1 Material parameters of the numerical modeling

Bulk parameters	Value	Cohesive parameters	Value
E	42 GPa	σ_c	300 MPa
ν	0.2	G_c	100 J/m^2
ρ	2,500 kg m^{-3}	Randomness on σ_c	10%

2.3 Results normalization

The material properties assigned to all the examples presented in this paper are detailed in Table 1.

To reproduce the defects, we add to the value of σ_c a random part that can reach up to 30 MPa (i.e. 10% of σ_c). The percentage of randomness on σ_c follows an uniform distribution. The weakest edges have consequently a strength of 300 MPa and the strongest ones 330 MPa.

These parameters do not refer to any specific material, which is not problematic since our results will be generally presented in adimensional form, i.e. independent of material parameters.

Three reference parameters have to be defined s_0, t_0 and $\dot{\varepsilon}_0$, respectively the characteristic length, time and strain rate. s_0 represents the size of a fragment obtained in quasi-statics assuming that all the potential energy is converted into fracture energy. This length s_0 is directly related to the characteristic time t_0 defined by Camacho and Ortiz (1996). It is the time taken by the stress wave released by a cohesive element to fully encompass a length s_0. It is expressed:

$$t_0 = \frac{EG_c}{\sigma_c^2 c} \tag{7}$$

and then

$$s_0 = c * t_0 \tag{8}$$

The characteristic strain rate $\dot{\varepsilon}_0$ defined by in Drugan (2001), can be interpreted as the strain rate to apply in order to completely open a cohesive element within the time t_0. Its analytical expression is:

$$\dot{\varepsilon}_0 = \frac{\sigma_c}{Et_0} \tag{9}$$

Thereby, the normalized strain rate and fragment size are:

$$\bar{\dot{\varepsilon}} = \frac{\dot{\varepsilon}}{\dot{\varepsilon}_0} \tag{10}$$

$$\bar{s} = \frac{s}{s_0} \tag{11}$$

With the parameters of Table 1, the celerity of waves c is 4,098 ms^{-1}, which gives $s_0 = 46.7\,\mu\mathrm{m}$ and $\dot{\varepsilon}_0 = 6.2710^5\ \mathrm{s}^{-1}$.

2.4 Analysis in terms of number of fragments

The results presented in this paper are expressed in number of fragments. For 1D simulations, the number of fragments is simply determined by counting the number of broken edges. The average fragment size is obtained by dividing the length of the bar by the number of fragments.

For 2D, an algorithm has been developed to analyze the results of fragmentation. It detects every closed contour which is then considered as a fragment. The surface of each fragment is computed by the summation of the surface of every elements inside the fragment. For uniaxial computation the size of a fragment is obtained by dividing the surface of the fragment by the height of the bar. For plates under biaxial loading, we assume that the fragment is a square and define its size as the square root of the surface.

3 Quasi 1D bar in uniaxial tension: effects of secondary waves on damage evolution

3.1 Numerical set-up

The first example presented consists of a bar in uniaxial tension. The example is called quasi 1D because the bar modeled contains only one element in the thickness. In that way, no crack propagation is involved, only initiation and opening.

The bar has a length of 3 cm. The mesh size is determined by convergence issues.

In order to clearly illustrate the effect of obscured zones, we try to simplify as much as possible this first example. We consider the case of a bar under a rapid and uniform extension, i.e. the strain rate is, before cracking, uniform along the longitudinal axis. This case is often presented as the most simple for fragmentation analysis Drugan (2001). The uniform strain rate is obtained by applying as an initial condition a velocity in the longitudinal direction that varies linearly with x.

$$V(x) = \dot{\varepsilon}\left(x - \frac{L}{2}\right) \quad x \in [0; L] \tag{12}$$

Table 2 Results of the convergence study: number of fragments obtained with different mesh sizes for a strain rate of 5.10^4 and $2.10^5\ \mathrm{s}^{-1}$

Mesh size (μm)	$5.10^4\ \mathrm{s}^{-1}$	$2.10^5\ \mathrm{s}^{-1}$
100	277	277
50	305	503
25	304	463
10	310	463

The boundary condition applied is an increasing displacement on the $x = \pm L/2$, in agreement with the constant strain rate.

$$\delta(x) = \begin{cases} -\dot{\varepsilon}\frac{L}{2}t & \text{if } x = 0 \\ \dot{\varepsilon}\frac{L}{2}t & \text{if } x = L \end{cases} \tag{13}$$

The applied strain rate varies from $\dot{\varepsilon} = 10^3\ \mathrm{s}^{-1}$ to $4.10^5\ \mathrm{s}^{-1}$.

3.2 Mesh convergence issues

We conduct a convergence study for the 1D bar case in order to determine the element size that leads to mesh independency. Four different meshes are tested with mesh sizes going from 100 to 10 μm. The number of fragments obtained for two different strain rates is summarized in Table 2.

The convergence is obtained in 1D for an element size of 50 μm at $5.10^4\ \mathrm{s}^{-1}$ (which makes a total of 2,200 elements) and 25 μm at $2.10^5\ \mathrm{s}^{-1}$ (4,400 elements). The mesh size is therefore chosen as a function of the strain rate. However, for strain rates lower than $5.10^4\ \mathrm{s}^{-1}$, we keep the element size equal to 50 μm.

Later in this article, we study the case of the fragmentation a 2D bar and a 2D plate. The mesh sizes chosen are the ones that lead to convergence in 1D, i.e. 50 μm for the lowest strain rates and 25 μm for the highest ones. The convergence in 2D is more tricky to get than in 1D. Here, our results do not strictly reach of convergence since the dissipated energy keeps increasing while we refine the mesh. However, the number of fragments is small enough compared to the number of elements (average fragments contain from 100 to 200 elements). Thus, the fragmentation is not limited by the mesh. This observation is sufficient to validate our study about the obscuration zones hypothesis, as energy convergence is not absolutely necessary.

We can explain the increase of the dissipated energy while refining the mesh by the way the defects are introduced. We chose to fix a uniform distribution of defects (a 10% variation on σ_c), which means that if the mesh is refined, the number of weakest links increases. As a consequence, the number of completely or partially damaged edges increases and the dissipated energy as well. This effect becomes visible in 2D as a significant amount of energy may be dissipated within the fragments volumes. A way to avoid this problem would be to fix the number of defects as in Levy et al. (2011), but this is out of the scope of this article.

3.3 Analysis of the stress wave propagation inside a fragment without the obscured zone hypothesis

To illustrate the physics of fragmentation and the way it can be affected by the obscured zones hypothesis, we recount on Fig. 3 the stress history on an edge from the beginning of the computation to its failure. The crack studied has a specific location: it appears inside an already existing fragment which length is 200 µm. The strain rate applied $\dot{\varepsilon} = 5.10^3\,\mathrm{s}^{-1}$ is a low strain rate for the material parameters chosen.

We can observe on the stress curve that failure occurs after multiple wave reflections. The first two cohesive elements that delimit the fragment boundaries, break rapidly. Stress release waves propagate away from these cracks. When they reach the boundaries of the fragment, they are reflected into tensile stress waves that damage the cohesive element inside the fragment. These waves are the one we called *secondary waves* before. Failure is reached progressively, as one can see on the figure. Indeed the maximum stress attained at each cycle decreases and we can count 21 "tension-compression" cycles before the crack opens. Meanwhile, one can observe that from the moment the fragment is created (i.e. when the longitudinal stress starts to decrease), stresses on the y-direction appear. It is due to the vibration of the fragment. The stress state in not perfectly 1D anymore, which can explain the small variations on the maximum level of σ_{xx}.

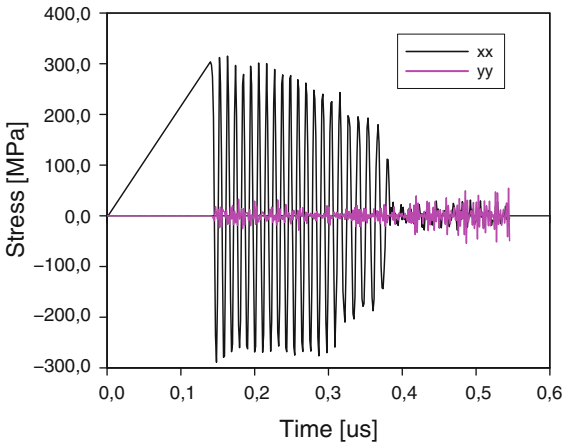

Fig. 3 Evolution of the normal (xx) and longitudinal (yy) stresses inside a fragment of 200 µm at 5000/s

If the obscured zone hypothesis would have been adopted in that case, the crack inside the fragment would not have opened, because the defect would have been protected from failure by the stress release wave that propagated just after the first two cracks opened.

3.4 Numerical measure of the obscured zone hypothesis influence

Now that the fragmentation process and the role played by the obscured zones have been made clearer, we can study the influence of the obscured zone hypothesis. In that aim, two sets of computation are carried out. The first one, with the standard cohesive method, as described in 2.1. is denoted thereafter *without obscuration*. The second one reproduces the hypothesis of the obscured zones as explained in 2.2 and will be called *with obscuration*.

Table 3 presents the number of fragments counted at the end of the computation. We considered the computation as finished when the dissipated energy does not evolve anymore. The fourth column is the percentage of difference between the two computations. The difference is computed as:

$$diff. = \frac{|Nb_{Frag}^{with\,obscuration} - Nb_{Frag}^{without\,obscuration}|}{Nb_{Frag}^{with\,obscuration}} * 100 \tag{14}$$

The difference is not limited to 100%, which would have happened if we divided the difference by the result without obscuration.

The results show that at high strain rates, considering or not the obscuration zones makes no difference. In this case, fragmentation is very fast, and the energy available is dissipated almost at once. The process is

Table 3 Number of fragments in a 1D bar under uniaxial tension. Influence of the obscured zone hypothesis on cracks initiation and fragmentation

Strain rate [s^{-1}]	With obscuration	Without obscuration	% of difference
1.10^3	60	141	135
2.10^3	85	151	77.7
5.10^3	130	178	36.9
1.10^4	175	207	18.3
2.10^4	213	234	9.9
5.10^4	303	309	2.0
1.10^5	339	335	1.2
2.10^5	463	458	1.1
4.10^5	630	632	0.3

governed by crack initiation (Levy et al. 2011) and we do not see the secondary waves described before. The lower the strain rate is, the more important the differences are observed. We can compute the velocity applied to the specimen by $v = \dot{\varepsilon} * l_{specimen}$. Given that the length of the bar is 3 cm and the wave celerity in the material is $c = 4{,}098\,\mathrm{ms}^{-1}$, the velocity of the loading is equal to the celerity of waves for a strain rate of $1.36\ 10^5 \mathrm{s}^{-1}$. This value corresponds to the strain rate at which the difference induced by the obscured zone hypothesis starts to be insignificant.

For higher strain rates, when the difference is small, we can observe a number of fragments obtained with obscuration higher than without. This is a numerical artifact due to the randomness introduced in σ_c. Therefore, it can be concluded that the use of the obscuration hypothesis always underestimates the final number of fragments.

As one can see on Fig. 4, the evolution of the difference as a function of the strain rate can be fitted by a function of type $y = \frac{1}{x}$, which is in fact related to the ratio between $\frac{c}{v}$, v being proportional to the applied strain rate.

Now we use the results to plot the average normalized fragment size as a function of the normalized strain rate (Fig. 5). We compare the results obtained by numerical simulation to the analytical ones from Grady (1982). They predict that the average normalized fragment size follows the law:

$$\overline{s} = \left(\frac{24}{\overline{\dot{\varepsilon}}^2}\right)^{2/3} \tag{15}$$

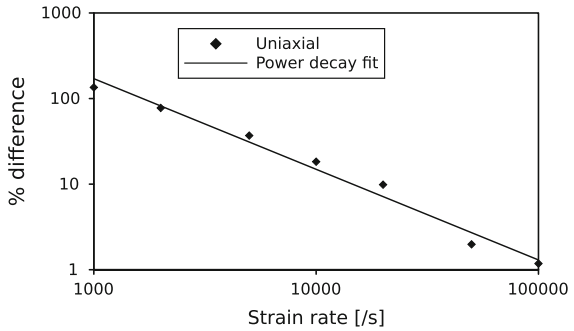

Fig. 4 Percentage of difference in the number of fragments between the models with and without obscured zones in a log-log plot. One can see that it follows a power decay

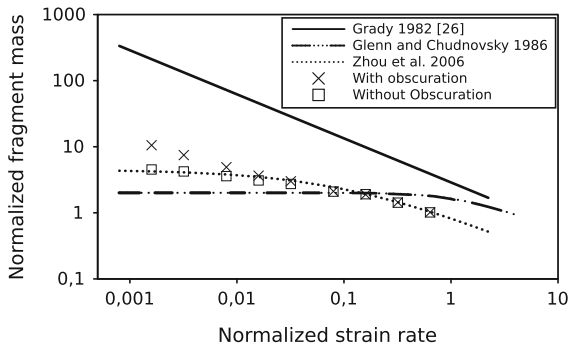

Fig. 5 Average normalized fragment size as a function of the normalized strain rate. Comparison of our numerical results to reference analytical ones. Normalization procedure is explained in Sect. 2.3

We also plot the law proposed by Glenn and Chudnovsky (1986):

$$\overline{s} = \frac{4}{\overline{\dot{\varepsilon}}\sinh\left(\frac{1}{3}\mathrm{asinh}(1.5\overline{\dot{\varepsilon}})\right)} \tag{16}$$

Finally, we recall the results from Zhou et al. (2006), obtained numerically with the cohesive elements:

$$\overline{s} = \frac{4.5}{1 + 4.5\overline{\dot{\varepsilon}}^{2/3}} \tag{17}$$

If we refer to the denominations introduced by Levy and Molinari (2010), we observe that the average fragments size predicted is not or slightly influenced by the obscured zone hypothesis in the "dynamic" and the "intermediate" regimes. The differences start to be important in the so-called "quasi-static" regime. The transition from the quasi-static to the intermediate regime happens for a normalized strain rate of about $10^{-2}\,\mathrm{s}^{-1}$ and we enter the dynamic regime at $\overline{\dot{\varepsilon}} \simeq 1\,\mathrm{s}^{-1}$.

4 Influence of the crack propagation process: 2D simulations in uniaxial and biaxial tension

Until now, we have explained the influence of the obscured zones on fragmentation, when only initiation is considered. Here, we make the problem more complex by introducing crack propagation. In that purpose, we study 2D examples: a bar of finite thickness in uniaxial tension and a plate in biaxial tension. The main difference between these two examples lies in the fact that in uniaxial tension, cracks propagate almost exclusively perpendicularly to the loading direction while in biaxial tension, they can propagate in any direction. As a consequence, there is mostly straight propagation in the first case whereas crack branching, bifurcation and coalescence can happen for biaxial loading. Each step of the formation of a fragment can be affected by the obscured zones hypothesis, in an even more influent manner due to the crack interactions. Obscured zones are now defined in a real 2D-space domain.

In the next section we describe in details the consequences of the interaction of obscured and cohesive zones.

4.1 2D bar in uniaxial tension

4.1.1 Numerical set-up

This example is similar to the previous one, the difference stands in the thickness of the bar. It is now made of eight elements in the thickness as shown in Fig. 6. The initial and boundary conditions are similar to the previous case.

4.1.2 An example of the interaction between obscured areas and cohesive zones

The cohesive zone is the domain in space where one can observe cohesive stress fields due to the presence of a crack tip or a notch. During crack propagation, under uniaxial loading the crack is most likely to propagate

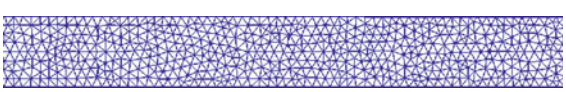

Fig. 6 Part of the mesh of the 2D bar for the uniaxial tension simulation

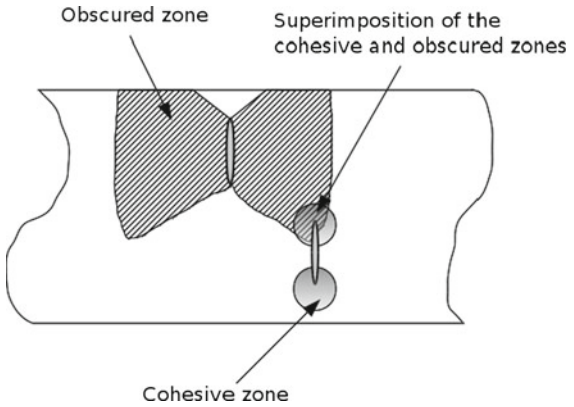

Fig. 7 Interaction between obscured and cohesive zones

straight, perpendicularly to the loading direction. However, due to the obscured zone theory, it is possible that an edge on the crack path has been made unbreakable because of the obscured zone created by another crack already initiated.

This case is illustrated in Fig. 7. When the cohesive zone and the obscured zone are superimposed, the crack cannot propagate anymore since no cohesive insertion is possible. It is however possible, that the crack follows another path, but sooner or later it may be blocked. After a while, the domain is completely obscured, the edges are then either *protected* or *broken*. At that point, the computation can be considered as finished, no more energy can be dissipated (see Forquin and Hild (2010), or statement recalled in Sect. 1.2). Depending on the strain rate, the total obscuration arises more a less soon in relation to the progress of the fragmentation process. The sooner it is, the more the results are affected. This point will be detailed in the next section, dedicated to the analysis of results.

4.1.3 Analysis of the results based on the number of fragments

Whatever the strain rate, we now observe a strong difference in the number of fragments (see Table 4). It decreases when strain rate increases. As explained in the previous section, the fragmentation process is blocked by the obscured zones when the reloading effect of the secondary waves is neglected. Nevertheless, for the "dynamic" regime, we can observe that the differences become reasonable. Levy et al. (2011) introduced the idea of a cross strain rate $\dot{\varepsilon}_{cross}$, at which, the fragmentation phenomenon passes from a strength

Table 4 Number of fragments in a 2D bar under uniaxial tension

Strain rate [s^{-1}]	With obscuration	Without obscuration	% of difference
1.10^3	1	40	3900
2.10^3 000	2	45	2150
5.10^3	3	52	1633
1.10^4	4	64	1500
2.10^4	5	87	1640
5.10^4	13	141	984
1.10^5	75	309	312
2.10^5	209	318	52.1
4.10^5	797	943	18.3

These results illustrate the influence of the obscured zone hypothesis on crack propagation

controlled regime to a toughness controlled one. For low and intermediate strain rates, the potential energy injected into the specimen is converted almost instantaneously into fracture energy. The time to failure is very small compared to the loading time. Relatively, the time to failure at high strain rate is longer. Since fracture happens relatively later at high strain rates, there are less interactions between the stress release and loading waves when the strain rate increases. As a consequence, the failure process is more independent of what is happening in the surroundings and becomes smoother. It is mainly controlled by the amount of energy to dissipate and then by the toughness of the material. At lower strain rates, the complex process of multiple reflections makes the cohesive strength the controlling parameter.

The cross point is defined as $\dot{\varepsilon}_{cross} = \frac{\dot{\varepsilon}_0}{2}$, which is for the material parameters used in this paper $\dot{\varepsilon}_{cross} = 3.13\ 10^5\ s^{-1}$.

It seems in this example, that this cross strain rate is also the strain rate at which the obscured zone hypothesis becomes suitable when crack propagation is involved.

4.2 2D plate in biaxial tension

4.2.1 Numerical set-up

We now study the case of a plate in uniform biaxial tension. The material properties are the same as before. A initial ramp of velocity is applied in both directions.

Table 5 Number of fragments resulting from the fragmentation of a 2D plate subjected to biaxial tension

Strain rate [s^{-1}]	With obscuration	Without obscuration	% of difference
1.10^3	1	45	4400
2.10^3	3	48	1500
5.10^3	4	65	1350
1.10^4	20	87	335
2.10^4	293	359	22.5
5.10^4	1020	1009	1.63
1.10^5	2737	2731	0.2

The plate is a square of $3 \times 3\,mm^2$ containing up to 185,000 elements for the highest strain rates.

4.2.2 Numerical results for a plate in biaxial tension

Table 5 shows the results obtained for the biaxial plate.

Two different regimes can clearly be identified: differences are large at low strain rate (*i.e.* for strain rates equal or lower than $10^4\ s^{-1}$) while they are in the same range of values for higher strain rates. It is now in the "quasi-static" and "intermediate" regimes that the differences are important, while in 1D, it was limited to the "quasi-static" one.

In biaxial tension, crack propagation is involved and is also strongly combined to crack coalescence. Indeed, cracks can now propagate in all directions, still favoring the directions perpendicular to the applied loading. The possibilities of crack propagation are more important as well as the chance that two cracks join together. Fragment generation is then facilitated.

Figure 8 illustrates how a fragment is created. We look at the stresses on the edge which closes in the end the fragment studied. Several observations can be made. First, the creation of a fragment takes a non negligible time, fragmentation cannot be considered as instantaneous. If we follow the evolution of the stress on this edge, we can see that it experiences multiple unloading and reloading, which would have made it unbreakable with the obscured zone modeling. Once again, secondary waves exist and play an important role.

If one now looks more precisely at the process, we can see, that first (step 1), damage initiates at different locations, due to the presence of defects. At step 2, crack initiation continues. The first edge breaks at step 3

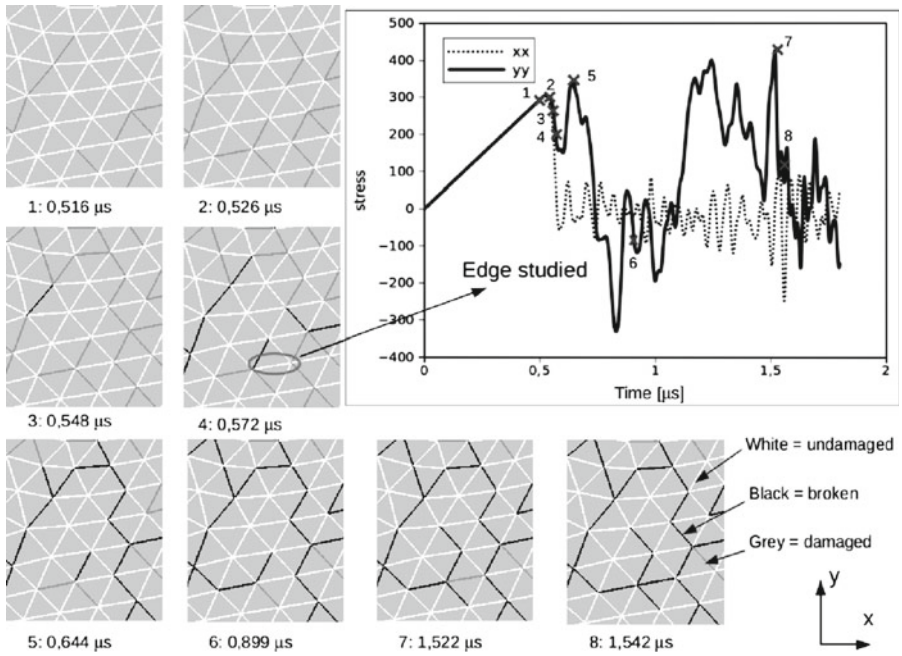

Fig. 8 History of a fragment at $\dot{\varepsilon} = 5.10^3\ s^{-1}$. The edges in white are undamaged, the ones in grey partially damaged and the black ones are broken. The stresses plotted are the average of the stresses computed in the x and y direction at the four Gauss points of the bulk elements neigboring the edge. Therefore, these stresses can exceed σ_c

and crack propagation happens at step 4. At steps 5 and 6, the different cracks initiated coalesce and one starts to see the borders of the future fragment. At step 6, only one broken edge is missing to form the fragment. The breakage of this last edge happens only much later at stage 8 ($t = 1.542\,\mu s$).

This example shows that the obscured zone hypothesis is not correct when the fragmentation process implies propagation and coalescence, phenomena that are not observed in 1D and that are not instantaneous.

If we compare the results to the ones obtained before, we observe that at high strain rates the obscured zone hypothesis is accurate, while it was not for the 2D bar. For instance at a strain rate of $1.10^5\ s^{-1}$, the difference in terms of number of fragments with and without obscuration is 3% for the biaxial tension versus 312% for the uniaxial one. However for low strain rate, this difference remains large, for instance it is 4,400% at $1.10^3\ s^{-1}$.

These two 2D examples showed that for low and intermediate strain rates, the use of the obscured zone hypothesis leads to important errors, that we explained by the interaction between cohesive and obscuration zones. As a consequence, the fragmentation is blocked and the entire domain is quickly obscured.

5 Influence of the material parameters

5.1 Numerical set-up

The example chosen to study the influence of the material parameters is the plate in biaxial tension. We focus on two properties: the distribution of defects and fracture toughness.

5.2 Numerical results for three different distributions of defects

As explained before, the heterogeneity of the material is reproduced by introducing a part of randomness on σ_c, the critical stress of each cohesive element. The distribution of this random part is uniform and could reach 10%. We now compare other distributions of σ_c, still uniform, but of different standard deviation: in one case it reaches 25%, and in the other one, only 2%. The way these new distributions affect the final number of fragments and the total energy dissipated with and without obscured zones is plotted in Fig. 9a and b.

As before, the obscured zone hypothesis is not harmful for high strain rates and not accurate for low strain

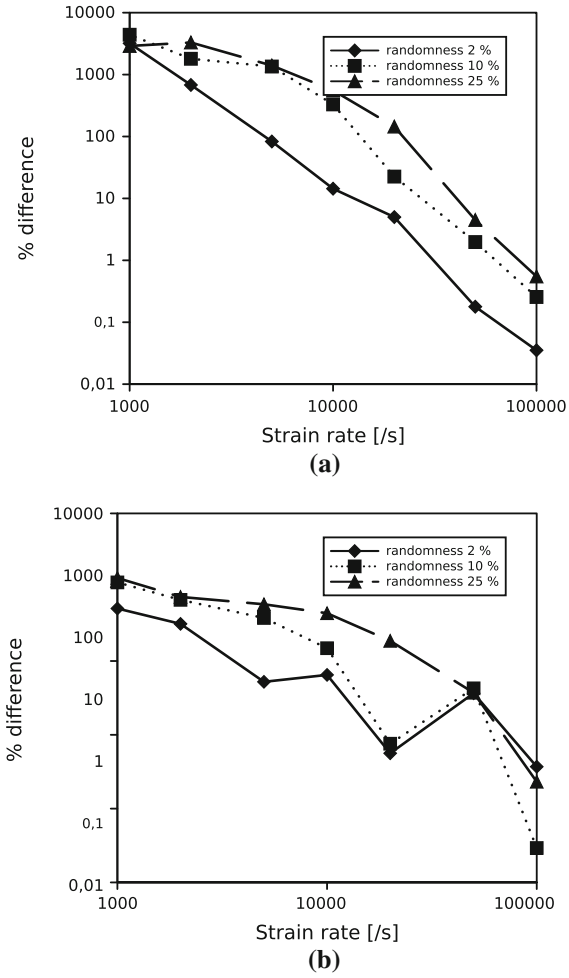

Fig. 9 (**a**) Number of fragments, (**b**) dissipated energy. Evolution as a function of strain rate of the differences computed with and without obscured zones, for three different values of randomness on σ_c. Plots in a log-log scale

rates. The distribution of defects has a visible effect for intermediate strain rates where one can see that the smaller the distribution is, the less differences one observes with or without obscured zones.

With a reduced distribution of defects and due to the uniform stress state, more defects are initiated at the same time. The fragmentation process is therefore more governed by crack initiation than propagation. As it has been shown before, crack initiation is less sensitive to the obscured zone modeling than propagation. On the opposite, with a large distribution of defects, few defects are initiated at once. Then, there is a competition between propagation of the cracks and of the stress release wave. We could observe previously that, in that case, obscured zones were strongly limiting the formation of fragments. The results observed here are in agreement with the previous conclusions.

Table 6 Number of fragments in a 2D plate under biaxial tension with $G_c = 25$

Strain rate [s^{-1}]	With obscuration	Without obscuration	% of difference
1.10^3	1	126	6200
2.10^3	3	135	4400
5.10^3	4	158	3850
1.10^4	11	201	1727
2.10^4	114	393	244
5.10^4	1201	1371	14
1.10^5	2604	2682	3

The analysis of the results of the dissipated energy brings us another piece of information. First, the differences induced by the obscured zones modeling are much less significant. We can also compare the strain rate at which these differences become important. Let us consider arbitrarily that results are in agreement if the difference is lower than 10%, and look at differences computed for a 10% variation on σ_c. We can see that in terms of dissipated energy, the results are valid for strain rates above $2.10^4\ s^{-1}$ while for the number of fragments it is only from $5.10^4\ s^{-1}$. This implies that at $2.10^4\ s^{-1}$, the number of broken edges remain equivalent but they do not manage to link up to make a fragment. Once again, we notice that crack propagation is more sensitive to the obscured zones than crack initiation.

5.3 Influence of the fracture toughness

The last point studied in this paper is the influence of the brittleness of the material. In that purpose, we conduct the same set of numerical simulations but we use a different value of the toughness G_c. Instead of chosing 100 J/m, we now have 25 J/m. The results are presented in Table 6. They have to be compared to the ones of Table 5.

The differences as a function of the strain rate are plotted in Fig. 10a and b. We also plot the differences observed in the dissipated energy.

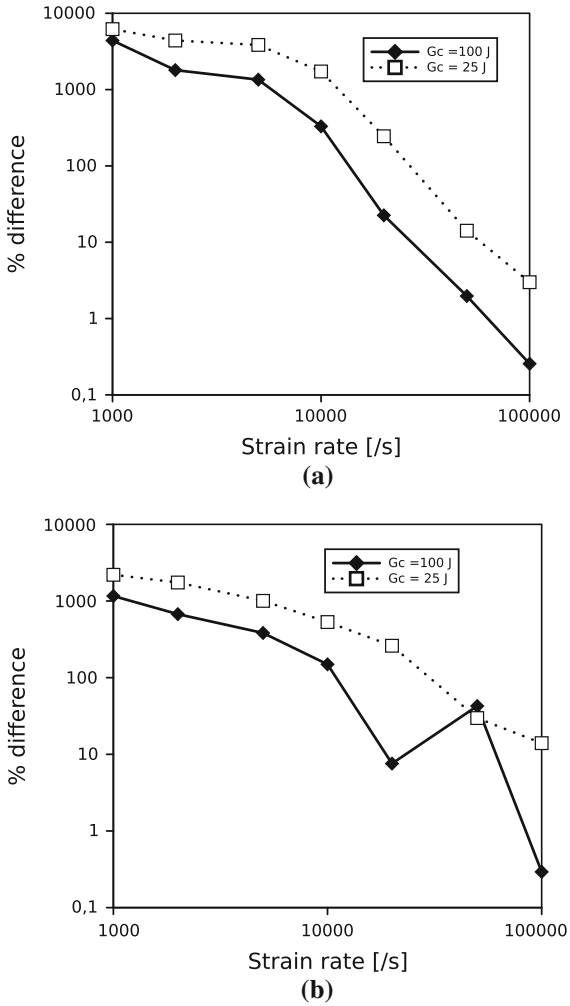

Fig. 10 (**a**) Number of fragments, (**b**) dissipated energy. Evolution as a function of strain rate of the differences computed with and without obscured zones, for two different values of G_c. Results of Tables 5 and 6. Plots in a log-log scale

The simulations show that a more brittle material is more affected by the obscured zones. If we reduce G_c, the cohesive elements break more quickly, and therefore frees the stress release wave before. As a consequence, the material is obscured faster than if the toughness is higher. The fragmentation process ends before.

The obscured zone hypothesis is as shown before affected by the time to crack opening. The shorter this time is and the more errors are made by using this hypothesis. A smaller G_c reduces this time and therefore affects the accuracy of the results when obscuration zones are modeled.

6 Conclusions

In this paper, we studied by the use of numerical modeling the obscured zone hypothesis that states that the fragmentation process ends when all the domain has been obscured by stress release waves. The influence of various parameters have been studied: the strain rate, the dimensionality of the problem, the phenomena involved in the fragmentation process, the toughness and the distribution of defects.

In general, it can be concluded that the obscuration hypothesis yields to an under-estimation of the number of fragments.

We observe that the obscured zone hypothesis provides accurate results when the fragmentation process is fast or instantaneous. This is the case when it is only controlled by crack initiation and not propagation. The examples that give good results are then the computations performed in quasi 1D, or with a quasi-homogeneous material. When the difference between the material velocity and the wave celerity is reduced, i.e. at high strain rates, the obscured zones hypothesis does not hamper the accuracy of the results. In that case, the loading stress propagates faster the stress release waves, which as a consequence does not affect fragmentation.

On the contrary, the hypothesis does not seem to hold when the fragmentation process implies cracks propagation, as for instance in the 2D bar in uniaxial tension. This effect is attenuated when the fragmentation process is more complex, and then the possibilities that cracks propagate in different directions and merge are more numerous.

For high strain rates, the accuracy of the obscured zone hypothesis should be mitigated by the fact that, in that case we expect the fragmentation to happen before obscuration takes place. There, models based on either energetic or statistic arguments are also accurate.

The obscuration-zone assumption is meant to deal then with lower strain rates, when the time-dependency of the phenomenon is important, and the fragmentation not instantaneous.

We showed in this paper that obscuration of defects does occur as we actually measure a decrease in the stress in the neighborhood of a crack just after its opening. It protects for a while a defect situated in that area. But the defect can be later reloaded by a secondary wave, and it that case, obscuration only introduces a delay in the fragmentation process. We demonstrated

that neglecting these secondary waves leads to important errors. As a consequence, the obscuration assumption should be corrected by giving to the obscuration of defects a life span that would depend on the wave speed and the size of fragments.

References

Astrom JA, Linna RP, Timonen J, Moller PF, Oddershede L (2004) Exponential and power-law mass distributions in brittle fragmentation. Phys Rev E 70(2) 026104

Camacho GT, Ortiz M (1996) Computational modelling of impact damage in brittle materials. Int J Solids Struct 3(20–22):2899–2938

Denoual C, Barbier G, Hild FA (1997) Probabilistic approach for fragmentation of ceramics under impact loading. C.R. Acad Sci Paris IIb 325:685–691

Donzé FV, Bouchez J, Magnier SA (1997) Modeling fractures in rock blasting. Int J Rock Mech Min Sci 34(8):1153–1163

Drugan WJ (2001) Dynamic fragmentation of brittle materials: analytical mechanics-based models. J Mech Phys Solids 49(6):1181–1208

Forquin P, Hild F (2010) A probabilistic damage model of the dynamic fragmentation process in brittle materials. Adv Appl Mech 44:1–72

Glenn LA, Chudnovsky A (1986) Strain-energy effects on dynamic fragmentation. J Appl Phys 59:1379–1380

Grady DE, Kipp ME (1985) Geometric statistics and dynamic fragmentation. J Appl Phys 83(3):1210–1222

Grady DE (2006) Fragmentation of rings and shells: the legacy of N.F. Mott. Springer, Berlin

Grady DE, Kipp ME, Benson DA (1984) Energy and statistical effects in the dynamic fragmentation of metal rings. Proc Conf Mech Prop High Rates Strain 70:315–320

Grady DE (1982) Local inertial effects in dynamic fragmentation. J Appl Phys 53(1):322–325

Herrman HJ, Wittel FK, Kun F (2006) Fragmentation. Physica A 371:59–66

Hughes T (2000) The finite element method: linear static and dynamic finite element analysis. Dover Publications, New York

Kipp ME, Grady DE (1985) Dynamic fracture growth and interaction in one dimension. J Mech Phys Solids 33(4):399–415

Levy S, Molinari JF (2010) Dynamic fragmentation of ceramics, signature of defects and scaling of fragment sizes. J Mech Phys Solids 58(1):12–26

Levy S, Molinari JF, Radovitzky R (2011) Dynamic fragmentation of a brittle plate under biaxial loading: strength or toughness controlled? Int J Numer Methods Eng (submitted)

Lienau CC (1936) Random fracture for brittle solid. J Franklin Inst 221:485–494

Maiti S, Rangaswamy K, Philippe H, Geubelle PH (2004) Mesoscale analysis of dynamic fragmentation of ceramics under tension. Acta Mater 53(3):823–834

Miller O, Freund LB, Needleman A (1996) Modeling and simulation of dynamic fragmentation in brittle materials. Int J Fracure 96(2):101–125

Mott NF, Linfoot EH (1943) A theory of fragmentation. Ministry of supply AC3348

Mott NF (1947) Fragmentation of shell cases. Proc Royal Soc A189:300–308

Morris JP, Rubin MB, Block GI, Bonner PM (2006) Simulations of fracture and fragmentation of geologic materials using combined FEM/DEM analysis. Int Impact Eng 33(1–12): 463–473

Rosin P, Rammler E (1999) The laws governing the fineness of powdered coal. J Inst Fuel 7:29–36

Weibull W (1951) A statistical distribution function of wide applicability. J Appl Mech 18:293–297

Weibull W (1939) A statistical theory of strength of materials. The Royal Swedish Institute of Engineering Research (Ingenors Vetenskaps Akadiens Handligar) Proceeding No. 151

Zhou F, Molinari JF, Ramesh KT (2006) Analysis of the brittle fragmentation of an expanding ring. Comput Mater Sci 37(1–2):74–85